This is a postprint of: Cement and Concrete Composites 33 (2011) 644 - 652

CORROSION BEHAVIOUR OF A NEW LOW-NICKEL STAINLESS STEEL EMBEDDED IN ACTIVATED FLY ASH MORTARS

M. Criado,[1*] D. M. Bastidas,[1] S. Fajardo,[1] A. Fernández-Jiménez,[2] and J. M. Bastidas[1]

[1] CENIM-National Centre for Metallurgical Research, CSIC, Avda. Gregorio del Amo 8, 28040 Madrid, Spain

[2] IETCC-Eduardo Torroja Institute of Construction Sciences, CSIC, Serrano Galvache 4, 28033 Madrid, Spain

M. Criado: mcriado@cenim.csic.es

D. M. Bastidas: david.bastidas@cenim.csic.es

S. Fajardo: s.fajardo@cenim.csic.es

A. Fernández-Jiménez: anafj@ietcc.csic.es

J. M. Bastidas: bastidas@cenim.csic.es

[*] Corresponding author, Tel.: +34 91 553 8900; Fax: +34 91 534 7425;

E-mail Address: mcriado@cenim.csic.es (M. Criado)

ABSTRACT

The present paper studies the corrosion behaviour of alkali-activated fly ash (AAFA) mortars manufactured using two alkaline solutions, with and without chloride additions (0.4% and 2%) in an environment of constant 95% relative humidity. Measurements were performed at early age curing up to 180 days of experimentation. A new, lower-cost type of austenitic stainless steel (SS) with a low nickel content was

studied. Conventional austenitic AISI 304 SS and carbon steel rebar were also tested for comparative purposes. The evolution with time of corrosion potential, polarization resistance and electrochemical impedance spectroscopy were studied.

Key Words: Low-nickel stainless steel; reinforced concrete; alkali-activated fly ash mortar; EIS; chloride addition

1 INTRODUCTION

The very high temperatures (~1500 ºC) required to manufacture ordinary Portland cement (OPC), which make it responsible for 40% of all energy consumed (~4000 kJ per kg of cement), account for the extremely high costs of this process [1]. The cement industry is regarded to be responsible for 6-7% of all greenhouse gases emitted world-wide (0.85-1 tonne of CO_2 per tonne of cement) [2]. Thus the construction sector is very interested in the development of new cement binder materials as an alternative to OPC. In this respect the most promising emerging approach is based on raw materials suitable for alkaline activation, essentially alkali-activated fly ash (AAFA), which is the origin of new binding materials generically known as alkaline cements [3-8].

Use of fly ash as a partial replacement material has become common practice in recent years [9-12]. Fly ash is used in concrete for reasons related with environmental impact, economic sustainability and social responsibility. The alkali activation of type F fly ash consists of mixing the ash with highly alkaline solutions (pH>13) and subsequently curing the resulting paste at a certain temperature to produce a solid material. In the ensuring chemical process, the vitreous structure that characterizes most of the particles is transformed into a compact cementitious material identified by its

excellent binding capabilities, mechanical strength development, feature high-volume stability, high fire resistance, and high durability in aggressive environments [13,14].

Steel rebars embedded in concrete are protected from corrosion by a thin oxide layer that is formed and maintained on their surfaces because of the highly alkaline environment of the surrounding concrete, with a pH usually in the range 12.5-13.5 [15]. However, with time, severe corrosion may occur in reinforced concrete structures (RCS). Corrosion is most frequently induced by the entry of chloride ions, leading to local destruction of the oxide layer. Chloride ions are commonly found in construction materials and may originate from the external environment, as in the case of marine environments, de-icing salts and acid rain [16].

Considering that reinforcement corrosion is the main cause of RCS failure [17], the capacity of an AAFA mortar to passivate steel rebars is a very important property to guarantee the durability of RCS constructed using these new materials. The passivating capacity and the permanence of the passive state once reached may depend on the nature and the dosage of the binder, the type of activator used and the environmental conditions.

Stainless steel (SS) reinforcements were first used many decades ago and have proved their ability to prevent corrosion for a very long time, even in very aggressive environments [18]. SS offers exceptional advantages for certain applications in construction and combines intrinsic durability with aesthetics, strength, ductility and formability. However, their use has been limited due to the high cost of SS compared to carbon steel. For this reason, new SSs, in which the nickel content has been lowered by replacement with other elements (nickel is subject to considerable price fluctuations due to stock market factors), are being evaluated as possible alternatives to conventional

carbon steel. This new low-nickel SS could mean a saving of about 15-20% compared to conventional AISI 304 SS.

Low-nickel austenitic SSs exhibit attractive properties that are comparable to those of traditional austenitic SSs, such as good corrosion resistance, high levels of strength and ductility and reduced tendency of grain sensitization [19]. Finally, the use of low-nickel austenitic SSs could be one of the most reliable methods to assure the durability of reinforced concrete structures exposed to aggressive environments [20]. Previous researches [21,22] have shown that the carbon steel corrosion rate values are similar to those of the traditional and low-nickel austenitic SSs in mortar without chloride additions, and at least 10 times higher in the presence of chloride. Futhermore, these SSs have had a corrosion behaviour very similar to that of traditional austenitic SSs in carbonated media and non-carbonated, chloride contaminated media [23].

The aim of this paper is to study the corrosion behaviour of a new type of austenitic SS, with a low nickel content, embedded in AAFA mortar with different chloride additions. Conventional austenitic AISI 304 SS and carbon steel are also studied for comparative purposes. Corrosion potential, polarization resistance and electrochemical impedance spectroscopy measurements have been performed to evaluate the corrosion behaviour of AAFA mortars at early age curing, up to 180 days of experimentation.

2 EXPERIMENTAL

2.1 Materials

Class F fly ash from the thermal power plant at Aboño in Asturias, Spain, was used [24]. Table 1 indicates its chemical composition. The percentage of reactive silica (SiO_2), determined according to UNE 80-225-93 [25], was 41.23%. The vitreous phase content in the fly ash was 65.60%. The procedure was similar to that described

elsewhere [26]. Briefly, 1 g of fly ash was added to 100 ml of 1% hydrofluoric acid (HF) in a plastic beaker and stirred for 6 h at room temperature. The granulometry distribution obtained by laser ray diffraction showed only one mode, where approximately 85% of particles were sized lower than 45 μm and 50% lower than 13 μm.

The fly ash was activated with two different highly alkaline solutions with roughly the same sodium oxide (Na_2O) content (~20%), but varying proportions of soluble SiO_2. The products used to prepare the solutions were laboratory grade reagents: PA-ACS-ISO, 98% sodium hydroxide (NaOH) pellets supplied by Panreac, and waterglass (Na_2SiO_3) (density of 1.38 g cm^{-3}) with the following composition: 8.2% Na_2O, 27% SiO_2 and 64.8% H_2O. The total silica content in the solutions was varied by adding different amounts of Na_2SiO_3 to the reaction media. The anion-type used in the activation reaction plays different roles: Whereas the hydroxyl ions act as a reaction catalyst during the activation process, on the other hand, the presence of silicate ions causes a reduction in the volume of pores within the system implying that there is an increase in the mechanical strength [27].

Austenitic low-nickel and AISI 304 SSs supplied by ACERINOX S.A. (a company in Cádiz, Spain) and carbon steel rebar were used as reinforcements for comparative purposes. Table 2 shows the chemical composition of the three materials.

2.2 Alkali Activation of Fly Ash

Two types of AAFA mortars were manufactured: one with a NaOH solution (AAFA1 specimen) and the other with a mixture of 85% NaOH and 15% waterglass (AAFA2 specimen) with a “liquid/solid” ratio of 0.45. The aggregate/AAFA ratio used to manufacture the mortars was 2. A standardised, evenly graded siliceous sand was employed (SiO_2 content of 99%, where 66% of particles with size <1 mm and 35% <0.5

mm). The moulds containing the fresh AAFA mortars were subsequently cured in an oven at 85 ºC in a saturated water vapour atmosphere for 20 h. Different amounts of sodium chloride (99% pure Panreac PRS-CODEX): 0, 0.4% and 2% Cl^- (with respect to binder weight) were added to fly ash. This compound was added to the fly ash that was subsequently mixed with the different alkaline solutions. Two mortar prism replicas of each type were prepared for comparative purposes. All the specimens were kept at room temperature in an atmosphere of high relative humidity (RH) of approximately 95%, for up to 180 days. .

2.3 Measurement Methods

Experiments were performed on small prismatic specimens measuring 8 × 5.5 × 2 cm, similar to those used in previous work [7]. Two 10-mm diameter, low-nickel SS, AISI 304 SS, and carbon steel rebar, symmetrically embedded in the prisms, were used as working electrodes during the measurements, with an external SS cylinder of 5 cm diameter acting as a counter electrode. The saturated calomel electrode (SCE) was the reference used in all potential measurements. A pad soaked in water was used to enable the electrical conductivity measurements. An active surface area of 5.6 cm^2 was marked on the working electrodes with adhesive tape, thus isolating the triple mortar/steel/atmosphere interface to avoid possible localised corrosion attack due to differential aeration.

Steel corrosion over time was monitored using three techniques: (i) corrosion potential (E_{corr}) values; (ii) linear polarization resistance (R_p) values ($R_p=\Delta E/\Delta I$); the steel corrosion current density (i_{corr}) can be calculated from the Stern-Geary equation [28]: $i_{corr}=B/R_p$, applying $\Delta E \pm 15$ mV at a scan rate of 0.16 mV s^{-1} and adopting a tentative value of 52 mV or 26 mV for the B constant for steel in the passive or active (corroding) state, respectively [29]; and (iii) electrochemical impedance spectroscopy

(EIS), EIS measurements were recorded at the E_{corr} in a frequency range from 64×10^{3} Hz to 1×10^{-2} Hz with a logarithmic sweeping frequency of 5 points per decade. The EIS method involved the imposition of a 10 mV amplitude excitation voltage. An EG&G PARC potentiostat model 273A and a 1250 Solartron frequency response analyser were utilised for R_p and EIS measurements. Electrochemical measurements were performed at 1, 7, 15, 30, 60, 90, 120 and 180 days.

Mercury intrusion porosimetry (MIP) has been employed for microstructural characterisation. MIP is based on Washburn's law: $D=(-4\cos\theta)\gamma/P$, where D is the pore diameter, θ the contact angle between the fluid and the pore mouth, γ the surface tension of the fluid, and P the applied pressure to fill up the pore with mercury (in this case the fluid). The surface tension for mercury at room temperature is 0.485 N m^{-1} and the contact angle employed was 141.3º. The porosimeter employed was an Autopore II 9220 by Micrometrics Instruments.

3 RESULTS

Figs. 1 and 2 show E_{corr} versus time for (a) low-nickel SS, (b) AISI 304 SS and (c) carbon steel rebar embedded in mortars AAFA1 and AAFA2 respectively, with different chloride additions (0, 0.4% and 2%). The specimens were kept at a high RH (~95%). As can be seen, in the absence of chlorides all the steel rebar exhibited E_{corr} values around −100 to −200 mV vs. SCE. The addition of chloride exerted different effects on the steel rebar. The E_{corr} values for low-nickel SS and AISI 304 SS were practically the same in mortars AAFA1 and AAFA2 in the absence and presence of chloride (see Fig. 1a-1b and Fig. 2a-2b). Carbon steel rebar embedded in mortar AAFA1 with 0.4% and 2% chlorides showed a decrease of 400 mV in the value of E_{corr} after 30 days experimentation (see Fig. 1c), indicating the active state. Nevertheless, carbon steel rebar embedded in mortar AAFA2 with 0.4% chloride remained in the

passive state (see Fig. 2c), but the mortar with 2% chloride presented a substantially more negative potential (~–500 mV vs. SCE), see Fig. 2c.

Figs. 3 and 4 show the i_{corr} values, estimated from the R_p measurements, versus time for (a) low-nickel SS, (b) AISI 304 SS and (c) carbon steel rebar embedded in mortars AAFA1 and AAFA2, respectively, with different chloride additions (0, 0.4% and 2%). In the absence of chlorides, all the steels exhibited i_{corr} values of the order of 0.01 µA cm^{-2}. The i_{corr} values on carbon steel embedded in mortar AAFA1 polluted with chlorides increased by two or three orders of magnitude, from 0.01 µA cm^{-2} to 1-10 µA cm^{-2}, see Fig. 3c. Also, it can be observed that the i_{corr} was ~100 times higher on carbon steel rebar embedded in mortar AAFA2 with 2% chloride (Fig. 4c) than in the same mortar without chlorides or with 0.4% chloride. Both SSs still exhibited i_{corr} values between 0.001-0.01 µA cm^{-2} in presence of chlorides.

Figs. 5, 6 and 7 show typical Nyquist plots for low-nickel SS, AISI 304 SS and carbon steel rebar respectively, embedded in mortars (a) AAFA1 and (b) AAFA2 with different chloride additions (0, 0.4% and 2%). Measurements were performed after 90 days of experimentation. In general, a capacitive behaviour was obtained, characterised by a poorly defined and depressed semicircle at high frequencies and a second semicircle at low frequencies. In the case of carbon steel rebar, a Warburg diffusion resistance element was defined after 90 days experimentation. Tables 3, 4 and 5 illustrate the fitting of impedance data for low-nickel SS, AISI 304 SS and carbon steel rebar, respectively, embedded in mortar AAFA1. Tables 6, 7 and 8 show the fitting of impedance data for low-nickel SS, AISI 304 SS and carbon steel rebar respectively, embedded in mortar AAFA2.

Tables 3-8 were yielded using the equivalent electrical circuit (EEC) of Fig. 8a (see below). It should be noted that for carbon steel rebar embedded in mortar AAFA1

with 0.4% or 2% chloride after 90 days experimentation, and in mortar AAFA2 with 2% chloride after 90 days experimentation, the EEC of Fig. 8b including a Warburg diffusion element was used in the fitting procedure (see Tables 5 and 8).

Fig. 9 shows total porosity results for mortars AAFA1 and AAFA2 after 90 days exposure to ~95% RH.

4 DISCUSSION

Figs. 1-4 obtained using the specimens manufactured with mortars AAFA1 and AAFA2 showed a certain similarity between the corrosion behaviour of low-nickel SS, AISI 304 SS and the carbon steel rebar in the absence of chlorides. These steels exhibited E_{corr} values around −100 to −200 mV vs SCE and i_{corr} values of the order of 0.01 μA cm^{-2}.

According to the results, the low-nickel SS and AISI 304 SS embedded in mortar AAFA1 with 0.4% and 2% chlorides (Fig. 1) showed E_{corr} values hundreds of millivolts higher (more noble) than the carbon steel rebar (~–500 mV vs. SCE). In contrast, the addition of 0.4% chloride did not cause a breakdown of passivity for the carbon steel rebar embedded in mortar AAFA2, see Fig. 2. The breakdown of passivity depends on the material characteristics to allow the diffusion of chlorides through its porous canal network [30]. A possible explanation for this behaviour was that the addition of a small amount of waterglass (15%) to the activating solution prompts the precipitation of a dense and compact reaction product [31], leading to a system with a slightly lower porosity (see Fig. 9), through a blocking and pore refinement process. Therefore, a lower porosity implies a greater difficulty in the mobility of chloride ions to the steel surface.

The evolution of i_{corr} over time (Figs. 3 and 4) shows differences in the i_{corr} value of around two or three orders of magnitude in the specimens with 0.4% and 2% chlorides. Using these chloride additions, carbon steel had lost its passivity and it corroded at high corrosion rates, i_{corr} = 1-10 μA cm^{-2}, except in mortar AAFA2 with chlorides additions of 0.4%, see Fig. 4, while the SSs, including the new low-nickel SS, still exhibited i_{corr} values of the order of 0.001-0.01 μA cm^{-2}.

Therefore, the new low-nickel SS does not present significant changes in E_{corr} and i_{corr} values, thus indicating the permanence of the passive state.

The EEC of Fig. 8a contains two distributed constant phase elements (CPE_{HF} and CPE_{LF}) to consider the two relaxation time constants (see Figs. 5-7). The CPE_{HF}-R_{HF} couple, which predominated at high frequencies, may be originated by the corrosion products formed over passive film in the mortars AAFA1 and AAFA2, while the CPE_{LF}-R_{CT} couple, controlling at low frequencies, characterises the corrosion process of double layer on the steel electrode. R_e was the electrolyte resistance [32]. Finally, the EEC of Fig. 8b contains two time constants (CPE_{HF}-R_{HF} and CPE_{LF}-R_{CT}) and a Warburg diffusion resistance element (W) (see Y_{0_W} parameter in Tables 5 and 8 for carbon steel rebar after 90 days experimentation). Concrete specimens subjected to chloride addition induces that the rebar embedded in them attains mixed migration and diffusion-controlled reaction. The coefficient of Warburg impedance in the Nyquist plot allows to predict the diffusion behaviour of chloride. A similar circuit was used by others authors [33,34] for chloride-induced corrosion of steel in concrete.

Distributed CPEs are widely used in data fitting to allow for depressed semicircles. This geometric feature is generally due to dispersion in the time constant caused by irregularities on the steel surface, surface roughness, fractal surface, and in general certain processes associated with an irregular distribution of the applied

potential. The admittance representation of a CPE (Y_{CPE}) shows a fractional-power dependent on the angular frequency (ω): $Y_{CPE}=Y_P(j\omega)^{\alpha}$, where Y_P is a real adjustable constant used in non-linear least squares (NLLS) fitting, and $-1<\alpha<1$ defined as a CPE power [35]. When $\alpha=0$, CPE is a resistor; when $\alpha=1$, it is an ideal capacitor; and when $\alpha=-1$, it is an inductor. Finally, if $\alpha=0.5$, CPE is the Warburg admittance.

Tables 3-5 include optimised fitting impedance parameter values for the AAFA1/steel system. The R_e values for three steels were in the range from 835 Ω cm^2 to 3466 Ω cm^2 for mortars without chloride and with 0.4% chloride, while they were lower (308 Ω cm^2) in the case of mortar with 2% chloride. This decrease in the R_e parameter may be attributed to a high concentration of free chloride ions in the pore network of the mortar, which enhance the electrical conductivity. At high frequency, a semicircle can be seen (Figs. 5a, 6a and 7a) which may be associated with the dielectric properties of the passive film. The high frequency process had a CPE_{HF} ($Y_{P_{HF}}$) in the range from 2 $\mu F cm^{-2} s^{-(1-\alpha_{HF})}$ to 17 $\mu F cm^{-2} s^{-(1-\alpha_{HF})}$. Passive layer resistance (R_{HF}) values from 149 Ω cm^2 to 752 Ω cm^2 were found in the absence of chlorides and with 0.4% chloride and from 21 Ω cm^2 to 108 Ω cm^2 for mortar with 2% chloride. Thus, the addition of a high chloride percentage originated a decrease in the R_{HF} parameter, suggesting that the passive film was not protective and its thickness was lower. Therefore, the mortar AAFA1 containing 2% chloride presented low corrosion resistance. Finally, at low frequencies a capacitive behaviour was observed, and the charge transfer resistance (R_{CT}), obtained from numerical fitting (see Tables 3-5), was as high as 35694 kΩ cm^2. R_{CT} values for low-nickel SS were very close to those of the AISI 304 SS. However, the presence of chlorides accelerated the corrosion process of carbon steel rebar, generating a decrease in the diameter of the semicircle and the shape of the EIS spectra shows noticeable change (see Fig. 7a). Also, R_{CT} values decrease

from 3282 kΩ cm^2 to 0.4 kΩ cm^2 and $Y_{P_{LF}}$ values increase from 22 μF$cm^{-2}s^{-(1-\alpha_{LF})}$ to 98 μF$cm^{-2}s^{-(1-\alpha_{LF})}$ at same time (see Table 5). During this process, the passive film has been destroyed by the chloride ion, thus indicating carbon steel has lost its passivity. Moreover, the EIS results show that the high concentration of chlorides will accelerate the diffusion process of species through the passive film. The Warburg diffusion process results from the diffusion of the chlorides through the steel/mortar interface. The Y_{0_W} shows an increasing tendency with the increasing of chloride ions, thus favouring mass transfer processes.

In previous work, it has been reported that the SS passive film present a duplex layer structure, whose inner layer is chromium oxide covered by an outer layer of iron oxide, where the nickel is found in the outer part of the film [36].

Accepting that the Stern-Geary equation can be applied, with an approximate B constant value of 52 mV or 26 mV, the resulting i_{corr} was 0.0021 μA/cm^2 and 1.73μA/cm^2, respectively, which were not far from the i_{corr} results obtained using lineal polarisation resistance measurements (see Fig. 3).

Tables 6-8 include optimised fitting impedance parameter values for the AAFA2/steel system. The high frequency process had a CPE_{HF} (Y_{PHF}) in the range from 2 μF$cm^{-2}s^{-(1-\alpha_{HF})}$ to 16 μF$cm^{-2}s^{-(1-\alpha_{HF})}$. The R_e and R_{HF} values for three steels were in the range from 295 Ω cm^2 to 1026 Ω cm^2 and from 17 Ω cm^2 to 250 Ω cm^2, respectively. A depressed capacitive semicircle was also observed at low frequency (see Tables 6-8), the R_{CT} values were extrapolated by fitting the low frequency portion of the diagram by a semicircle. These values were very high (~>10^4 kΩ cm^2), see Tables 6-8, the R_{CT} for SSs were similar. In contrast, the carbon steel rebar embedded in mortar AAFA2 with 2% chloride showed a semicircle that revealed a R_{CT} as low as 2 kΩ cm^2, indicating the

breakdown of the passive state. Under these conditions, a Warburg impedance developed at low frequencies, revealing a diffusion process of species when the initiation corrosion of the reinforcing steel had taken place. The Y_{0_W} shows a decreasing tendency in the time (see Table 8), indicating the diffusion of chloride is a time-dependent process. It will decrease with time since the capillary pore system will be altered as hydration products continue to form. In this mortar only a Warburg impedance in 2% chloride is observed; the pore constriction by pozzolanic reaction and chloride binding (form complex salts, Friedel`s salt) reduces the chloride diffusion towards the corrosion products layer.

Therefore, corrosion is a function of both the concrete and steel characteristics. It can be observed that the R_{CT} of the low-nickel SS very close to the charge transfer resistance the traditional AISI 304 SS in mortars AAFA1 and AAFA2 with 0.4% and 2% chloride additions. This suggests the very low corrosion susceptibility of the low-nickel SS reinforcements in these mortars. The effect caused by the reduced Ni-content is almost balance by the beneficial effect of other additives such as manganese or nitrogen, present in higher concentration than in AISI 304 SS. In the present study and in the literature [21,22], the influence of the metal base composition on the corrosion process has proved not to be a very important factor, and the low-nickel SS embedded in the AAFA1 and AAFA2 chloride-polluted mortars has a good durability.

5 CONCLUSIONS

Activated fly ash mortars provide a chemical protection to highly alkaline (pH>13) concrete pore solution, causing the passivation of steel reinforcements. The passive state stability depends on the activator employed and can also be affected by the environmental conditions.

The E_{corr} values for low-nickel were similar to those of the AISI 304 SSs in mortars AAFA1 and AAFA2 with and without chloride additions, with values of around -100 to -200 mV. In these mortars, low-nickel exhibited i_{corr} values of the order of 0.001-0.01 µA cm^{-2} in presence of chlorides. These results suggest a good durability of low-nickel SS embedded in fly ash mortars.

EIS results for low-nickel SS show two distributed time constants at high and low frequencies, attributed to the capacitive response of the passive film and the double layer, respectively.

ACKNOWLEDGEMENTS

M. Criado, D. M. Bastidas and S. Fajardo express their gratitude to the Spanish National Research Council (CSIC) for their contract under the JAE-Doc contract, the Ramón and Cajal Program and JAE-Predoc co-financed by the European Social Fund, respectively. The authors express their gratitude to Project BIA2008-05398 from CICYT, Spain, for financial support and to ACERINOX SA for providing the stainless steels utilized.

REFERENCES

1. García-Lodeiro I, Palomo A, Fernández-Jiménez A. Alkali-aggregate reaction in activated fly ash systems. Cement Concrete Res. 2007; 37:175-83.
2. Fernández-Jiménez A, Palomo A, López-Hombrados C. Engineering properties of alkali-activated fly ash concrete. ACI Mater. J. 2006;103:106-12.
3. Roy DM. Alkali-activated cements opportunities and challenges. Cement Concrete Res. 1999;29:249-54.
4. Palomo A, Gtutzeck MW, Blanco MT. Alkali-activated fly ashes: A cement for the future. Cement Concrete Res. 1999;29:1323-9.

5. Duxson P, Fernández-Jiménez A, Provis JL, Lukey GC, Palomo A, van Deventer JSJ. Geopolymer technology: The current state of the art. J. Mater. Sci. 2007;42:2917-33.
6. Wang SD, Scrivener KL. Hydration products of alkali activated slag cement. Cement Concrete Res. 1995;25:561-71.
7. Bastidas DM, Fernández-Jiménez A, Palomo A, González JA. A study on the passive state stability of steel embedded in activated fly ash mortars. Corros. Sci. 2008;50:1058-65.
8. Criado M, Fernández-Jiménez A, Palomo A. Effect of sodium sulfate on the alkali activation of fly ash. Cement Concrete Comp. 2010;32:589-94.
9. Choi YS, Kim JG, Lee KM. Corrosion behaviour of steel bar embedded in fly ash concrete. Corros. Sci. 2006;48:1733-45.
10. Montemor MF, Cunha MP, Ferreira MG, Simoes AMP. Corrosion behaviour of rebars in fly ash mortar exposed to carbon dioxide and chlorides. Cement Concrete Comp. 2002;24:45-53.
11. Saraswathy V, Muralidharan S, Thangavel K, Srinivasan S. Influence of activated fly ash on corrosion-resistance and strength concrete. Cement Concrete Comp. 2003;25:673-80.
12. Garcés P, Andión LG, Zornoza E, Bonilla M, Payá J. The effect of processed fly ashes on the durability and the corrosion of steel rebars embedded in cement-modified fly ash mortars. Cement Concrete Comp. 2010;32:204-10.
13. Van Jaarsveld JGS, van Deventer JSJ, Lukey GC. The effect of composition and temperature on the properties of fly ash and kaolinite-based geopolymers. Chem. Eng. J. 2002;89:63-73.
14. Fernández-Jiménez A, García-Lodeiro I, Palomo A. Durability of alkali-activated fly ash cementitious materials. J. Mater. Sci. 2007;42:3055-65.

15. Bertolini L, Elsener B, Pedeferri P, Polder R. Corrosion of steel in concrete-Prevention, diagnosis, repair. Ed. Wiley VCH, 2004.
16. Tommaselli MAG, Mariano NA, Kuri SE. Effectiveness of corrosion inhibitors in saturated calcium hydroxide solutions acidified by acid rain components. Constr. Build. Mater. 2009;23:328-33.
17. Gónzalez JA, Feliu S, Rodríguez P, Ramirez E, Alonso C, Andrade C. Some questions on the corrosion of steel in concrete. Part I: when, how and how much steel corrodes. Mater. Struct. 1996;29:40-6.
18. Castro-Borges P, de Rincón OT, Moreno EI, Torres-Acosta AA, Martínez-Madrid M, Knudsen A. Performance of a 60-year-old concrete pier with stainless steel reinforcement. Mater. Performance 2002;41:50-5.
19. Di Schino A, Barteri M, Kenny JM. Fatigue behaviour of a high nitrogen austenitic stainless steel as a function of its grain size. J. Mater. Sci. Lett. 2002;21:1969-71.
20. Baddoo NR. Stainless steel in construction: A review of research, applications, challenges and opportunities. J. Constr. Steel Res. 2008;64:1199-206.
21. García-Alonso MC, Escudero ML, Miranda JM, Vega MI, Capilla F, Correia MJ, Salta M, Bennani A, González JA. Corrosion behaviour of new stainless steels reinforcing bars embedded in concrete. Cement Concrete Res. 2007;37:1463-71.
22. García-Alonso MC, González JA, Miranda J, Escudero ML, Correia MJ, Salta M, Bennani A. Corrosion behaviour of innovative stainless steels in morta. Cement Concrete Res. 2007;37:1562-9.
23. Bautista A, Blanco G, Velasco F. Corrosion behaviour of low-nickel austenitic stainless steel reinforcements: a comparative study in simulated pore solutions. Cement Concrete Res. 2006;36:1922-30.

24. ASTM C 618-03 Standard, Standard specification for coal fly ash and raw or calcined natural pozzolan for use in concrete, Annual book for ASTM Standards, American for Testing and Materials (2003).
25. UNE 80-225-93 Spanish Standard, Test method for cements: chemical analysis. Determination of the reactive silica (SiO_2) content in cements, pozzolans and fly ashes (1993).
26. Arjuman P, Silbee MR, Roy DM. Quantitative determination of the crystalline and amorphous phases in low calcium fly ash. Ed. H. Justnes, In: Proc. 10th ICCC Gothenburg, Sweden, 3v 020 4p (1997).
27. Fernández-Jiménez A, Palomo A. Composition and microestructure of alkali activated fly ash binder: Effect of activator. Cement Concrete Res. 2005;35:1984-92.
28. Stern M, Geary AL. Electrochemical polarization I. A theoretical analysis of the shape of polarization curves. J. Electrochem. Soc. 1957;104:56-63.
29. Andrade C, Castelo V, Alonso C, González JA. The determination of the corrosion rate of steel embedded in concrete by the polarization resistance and AC impedance methods. In: STP 906, Corrosion of Rebar in Concrete, ASTM, Philadelphia, PA (1984).
30. Batis G, Pantazopoulou P, Tsivilis S, Badogiannis E. The effect of metakaolin on the corrosion behaviour of cement mortars. Cement Concrete Comp. 2005;27:125-30.
31. Fernández-Jiménez A, Palomo A, Criado M. Alkali activated fly ash binders. A comparative study between sodium and potassium activators. Mater. Construcc. 2006;56:51-65.
32. Feliu V, González JA, Andrade C, Feliu S. Equivalent circuit for modelling the steel-concrete interface. I. Experimental Evidence and theoretical predictions. Corros. Sci. 1998;40:975-93.

33. Montemor MF, Simoes AMP, Salta MM. Effect of fly ash on concrete reinforcement corrosion studied by EIS. Cement Concrete Comp. 2000;22:175-85.
34. Qiao G, Ou J. Corrosion monitoring of reinforcing steel in cement mortar by EIS and ENA. Electrochim. Acta 2007;52:8008-19.
35. Bastidas DM. Interpretation of impedance data for porous electrodes and diffusion processes. Corrosion 2007;63:515-21.
36. Fajardo S, Bastidas DM, Ryan MP, Criado M, McPhail DS, Bastidas JM. Low-nickel stainless steel passive film in simulated concrete pore solution: A SIMS study. Appl. Surf. Sci. 2010;256:6139–43.

FIGURE CAPTIONS

Fig. 1. Corrosion potential (E_{corr}) versus time for (a) low-nickel SS, (b) AISI 304 SS and (c) carbon steel rebar embedded in mortar AAFA1 for different chloride additions and exposed to a ~95% RH.

Fig. 2. Corrosion potential (E_{corr}) versus time for (a) low-nickel SS, (b) AISI 304 SS and (c) carbon steel rebar embedded in mortar AAFA2 for different chloride additions and exposed to a ~95% RH.

Fig. 3. Corrosion current density (i_{corr}) versus time estimated from the R_p measurements for (a) low-nickel SS, (b) AISI 304 SS and (c) carbon steel rebar embedded in mortar AAFA1 for different chloride additions and exposed to a ~95% RH.

Fig. 4. Corrosion current density (i_{corr}) versus time estimated from the R_p measurements for (a) low-nickel SS, (b) AISI 304 SS and (c) carbon steel rebar embedded in mortar AAFA2 for different chloride additions and exposed to a ~95% RH.

Fig. 5. Nyquist plots after 90 days experimentation for low-nickel SS rebar embedded in mortars (a) AAFA1 and (b) AAFA2 exposed to a ~95% RH.

Fig. 6. Nyquist plots after 90 days experimentation for AISI 304 SS rebar embedded in mortars (a) AAFA1 and (b) AAFA2 exposed to a ~95% RH.

Fig. 7. Nyquist plots after 90 days experimentation for carbon steel rebar embedded in mortars (a) AAFA1 and (b) AAFA2 exposed to a ~95% RH.

Fig. 8. Equivalent electrical circuit used to fit impedance data of steel embedded in mortars AAFA1 and AAFA2 and exposed to ~95% RH. R_e is the electrolyte/concrete interface resistance; CPE_{HF} and CPE_{LF} are constant phase elements defined at high and low frequency, respectively; R_{HF} is the mortar resistance; W is a Warburg diffusion component; and R_{CT} is the charge transfer resistance (corrosion).

Fig. 9. Total porosity results for mortars AAFA1 and AAFA2 after 90 days of ageing.

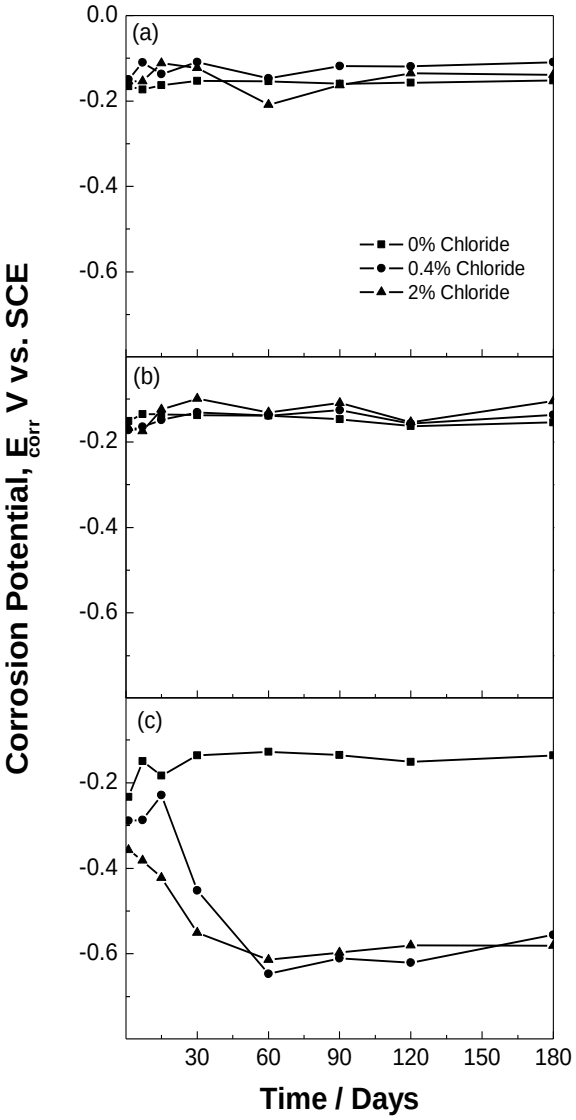
(a)
(b)
(c)
0% Chloride
0.4% Chloride
2% Chloride
0.0
-0.2
-0.4
-0.6
30
60
90
120
150
180
Time / Days
Corrosion Potential, E corr V vs. SCE

Figure 1.

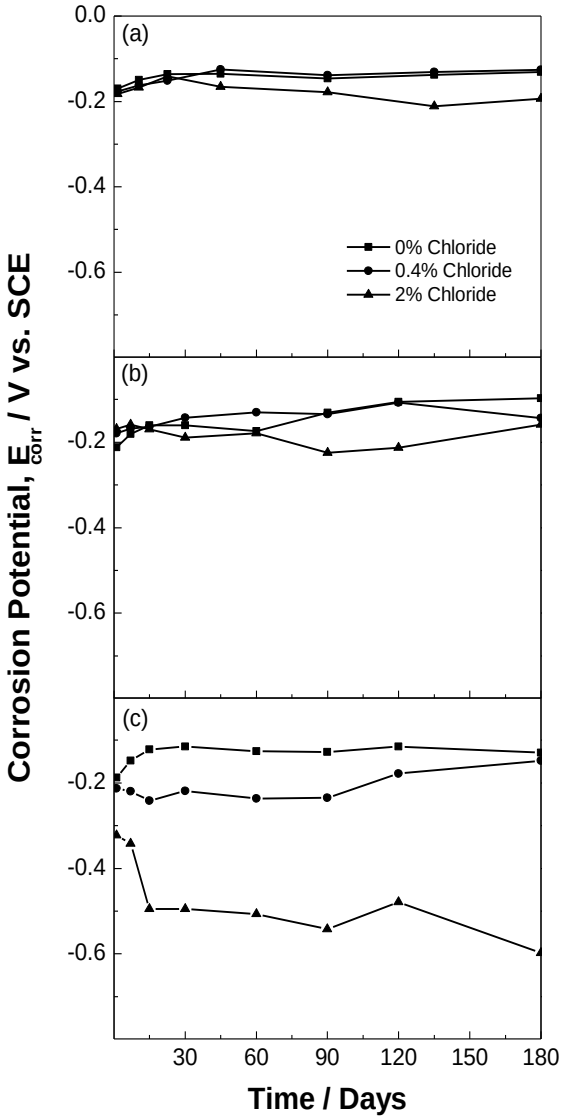
(a)
(b)
(c)
0% Chloride
0.4% Chloride
2% Chloride
0.0
-0.2
-0.4
-0.6
30
60
90
120
150
180
Time / Days
Corrosion Potential, E_corr / V vs. SCE

Figure 2

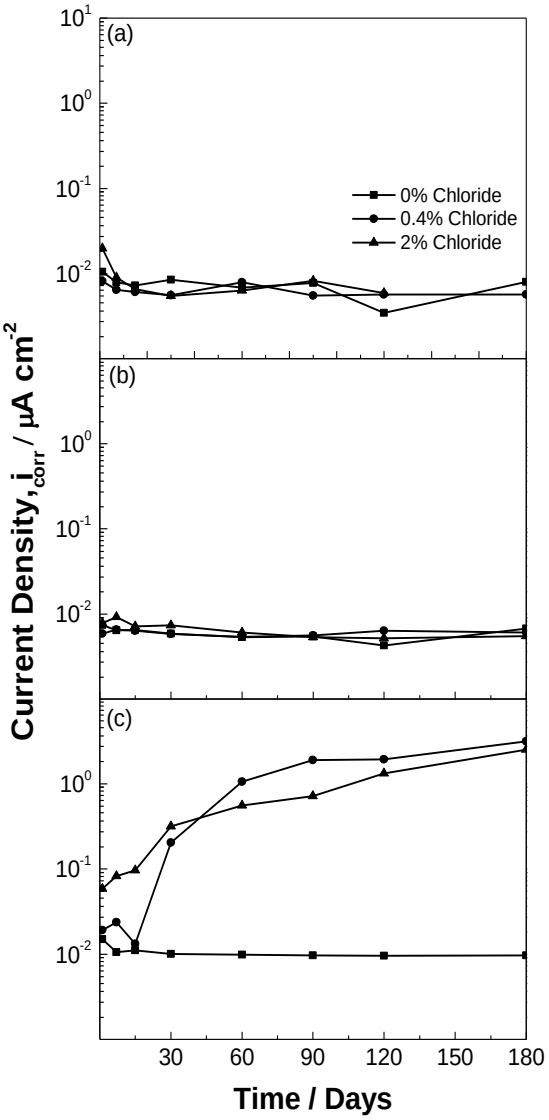
(a)
(b)
(c)
0% Chloride
0.4% Chloride
2% Chloride
Current Density, i_{corr} / μA cm^{-2}
Time / Days
10^{1}
10^{0}
10^{-1}
10^{-2}
30
60
90
120
150
180

Figure 3

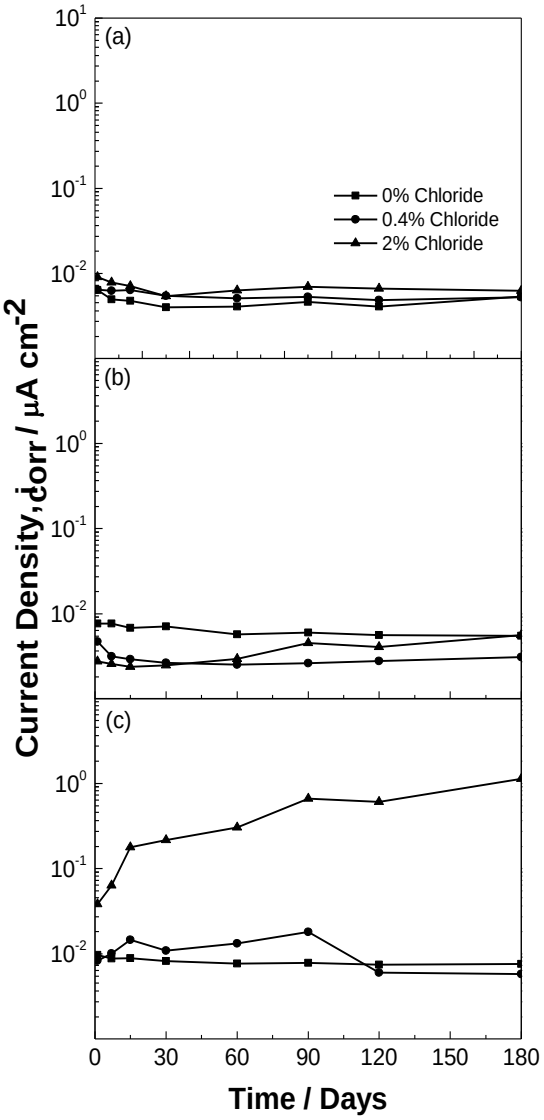
(a)
(b)
(c)
0% Chloride
0.4% Chloride
2% Chloride
Current Density, icorr / μA cm-2
Time / Days
0
30
60
90
120
150
180

Figure 4

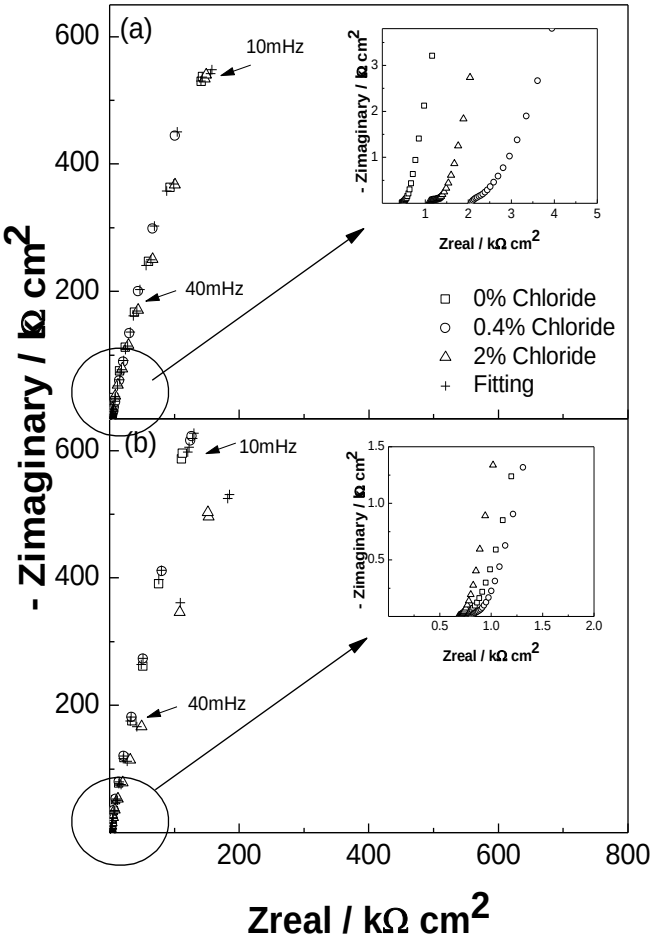
(a)
10mHz
40mHz
0% Chloride
0.4% Chloride
2% Chloride
Fitting
(b)
10mHz
40mHz
- Zimaginary / kΩ cm2
Zreal / kΩ cm2

Figure 5

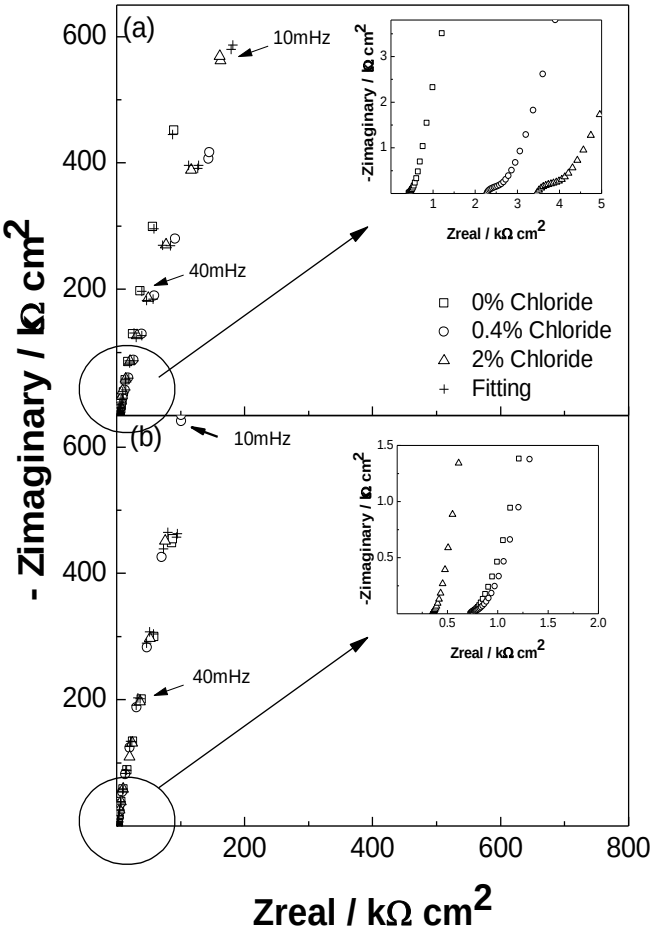
(a)
10mHz
40mHz
0% Chloride
0.4% Chloride
2% Chloride
Fitting
(b)
10mHz
40mHz
- Zimaginary / kΩ cm2
Zreal / kΩ cm2
-Zimaginary / kΩ cm2
Zreal / kΩ cm2

Figure 6

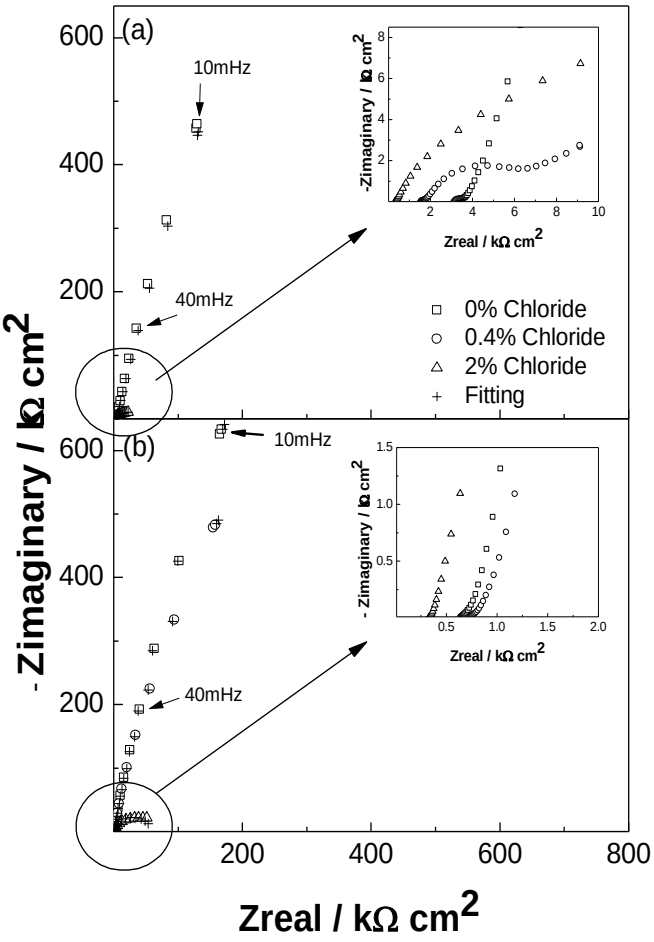
(a)
10mHz
40mHz
0% Chloride
0.4% Chloride
2% Chloride
Fitting
(b)
10mHz
40mHz
- Zimaginary / kΩ cm2
Zreal / kΩ cm2

Figure 7

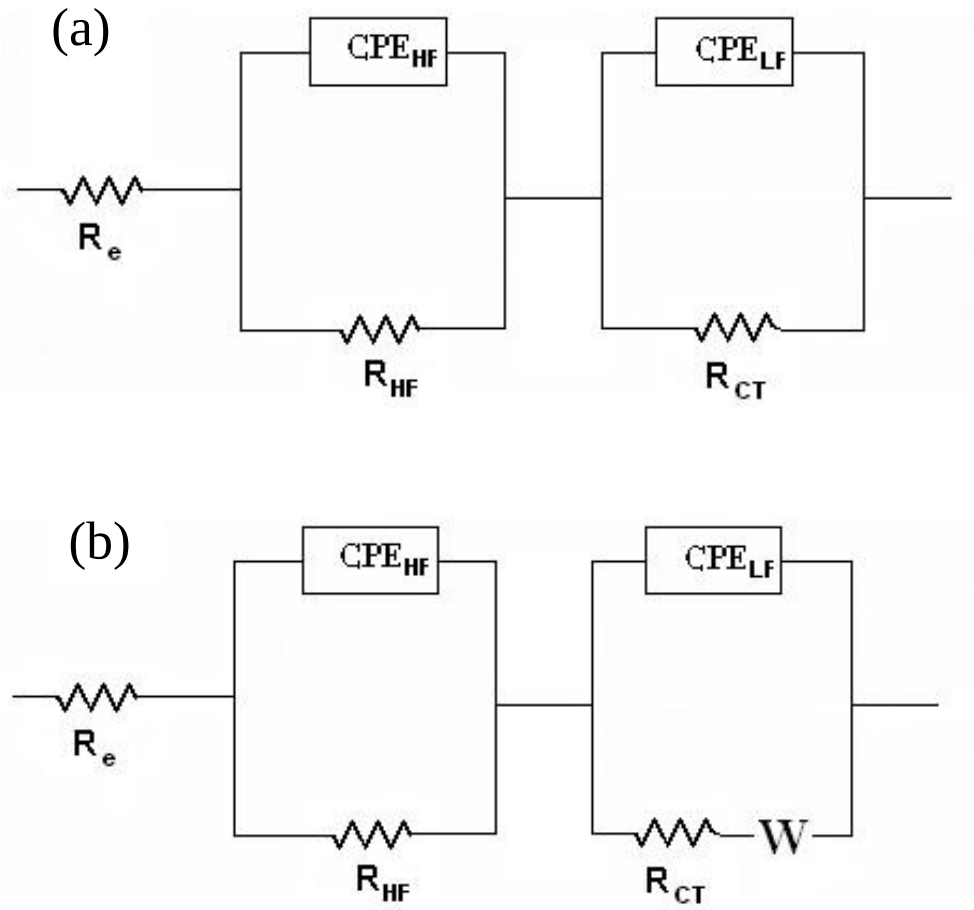

Figure 8

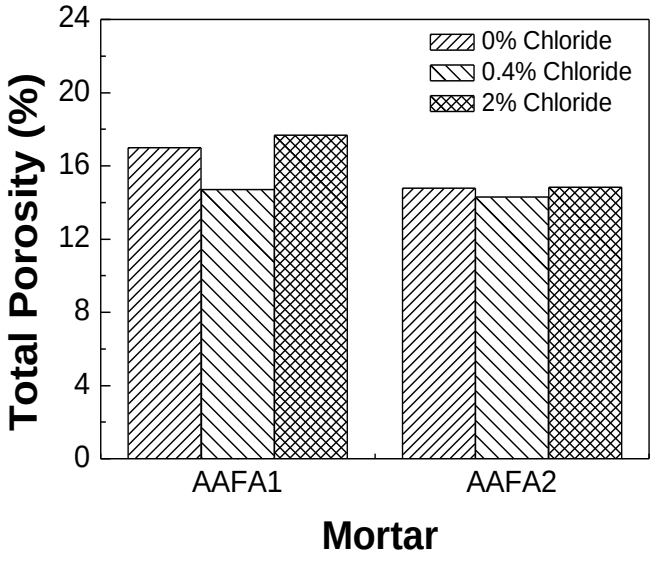
24
20
16
12
8
4
0
Total Porosity (%)
0% Chloride
0.4% Chloride
2% Chloride
AAFA1
AAFA2
Mortar

Figure 9

Tables

Table 1. Chemical composition of the tested fly ash (% in mass).

Table 2. Chemical composition (% by weight[a]) of the tested austenitic low-nickel SS, austenitic AISI 304 SS and carbon steel.

Table 3. Parameters used in the fitting of impedance data for low-nickel SS rebar embedded in mortar AAFA1.

Table 4. Parameters used in the fitting of impedance data for AISI 304 SS rebar embedded in mortar AAFA1.

Table 5. Parameters used in the fitting of impedance data for carbon steel rebar embedded in mortar AAFA1.

Table 6. Parameters used in the fitting of impedance data for low-nickel SS rebar embedded in mortar AAFA2.

Table 7. Parameters used in the fitting of impedance data for AISI 304 SS rebar embedded in mortar AAFA2.

Table 8. Parameters used in the fitting of impedance data for carbon steel rebar embedded in mortar AAFA2.

Table 1. Chemical composition of the tested fly ash (% in mass).

SiO_2	Al_2O_3	Fe_2O_3	CaO	MgO	SO_3	Na_2O	K_2O	MnO	P_2O_5	TiO_2	LOI	Others	Total
51.78	27.80	6.18	4.59	1.52	0.71	0.59	2.51	0.06	0.62	1.35	2.23	0.06	100

LOI: Loss on ignition.

Table 2. Chemical composition (% by weight[a]) of the tested austenitic low-nickel SS, austenitic AISI 304 SS and carbon steel.

Material	C	Si	Mn	P	S	Cr	Ni	Mo	Cu	N
Low-Nickel	0.082	0.48	7.26	0.027	0.001	16.56	4.32	0.07	0.13	0.075
AISI 304	0.049	0.32	1.75	0.028	0.001	18.20	8.13	0.22	0.21	0.059
Carbon Steel	0.45	0.22	0.72	<0.01	0.022	0.13	0.13	–	0.18	–

[a] The balance was Fe.

Table 3. Parameters used in the fitting of impedance data for low-nickel SS rebar embedded in mortar AAFA1.

Time Day	R_e Ω cm^2	$Y_{P_{HF}}$ μFcm^{-2}s$^{-(1-\alpha_{HF})}$	α_{HF}	R_{HF} Ω cm^2	$Y_{P_{LF}}$ μFcm^{-2}s$^{-(1-\alpha_{LF})}$	α_{LF}	R_{CT} kΩ cm^2
0% Chloride							
7	1738	4	0.65	407	21	0.86	4676
30	2078	4	0.67	422	20	0.86	13306
90	1026	4	0.63	305	20	0.87	9027
180	835	4	0.70	149	21	0.88	7942
0.4% Chloride							
7	1646	4	0.71	370	17	0.86	19684
30	1915	6	0.66	498	16	0.87	13390
90	2066	4	0.73	515	16	0.87	24578
180	2594	7	0.66	671	17	0.87	22764
2% Chloride							
7	347	7	0.69	50	19	0.88	9234
30	354	7	0.70	57	20	0.86	14146
90	450	8	0.70	74	19	0.86	9621
180	535	9	0.70	90	19	0.87	8121

Table 4. Parameters used in the fitting of impedance data for AISI 304 SS rebar embedded in mortar AAFA1.

Time Day	R_e Ω cm^2	$Y_{P_{HF}}$ μFcm^{-2}s$^{-(1-\alpha_{HF})}$	α_{HF}	R_{HF} Ω cm^2	$Y_{P_{LF}}$ μFcm^{-2}s$^{-(1-\alpha_{LF})}$	α_{LF}	R_{CT} kΩ cm^2
0% Chloride							
7	2492	2	0.73	511	18	0.88	17870
30	2632	4	0.67	596	18	0.89	24013
90	3466	2	0.72	677	17	0.89	35694
180	3331	4	0.67	752	18	0.89	25157
0.4% Chloride							
7	1529	4	0.75	282	17	0.87	9598
30	1979	4	0.71	417	15	0.87	19174
90	2271	4	0.71	462	24	0.83	10170
180	1936	6	0.69	451	16	0.87	13171
2% Chloride							
7	420	15	0.71	108	15	0.89	5522
30	414	12	0.65	72	16	0.87	7140
90	416	17	0.65	72	17	0.86	8070
180	493	2	0.83	56	18	0.83	12836

Table 5. Parameters used in the fitting of impedance data for carbon steel rebar embedded in mortar AAFA1.

Time Day	R_e Ω cm^2	$Y_{P_{HF}}$ μFcm^{-2}s$^{-(1-\alpha_{HF})}$	α_{HF}	R_{HF} Ω cm^2	$Y_{P_{LF}}$ μFcm^{-2}s$^{-(1-\alpha_{LF})}$	α_{LF}	R_{CT} kΩ cm^2	Y_{0_W} Ω^{-1} cm^{-2} s$^{1/2}$
0% Chloride								
7	2078	8	0.59	559	24	0.85	7974	–
30	2526	10	0.57	722	24	0.86	8557	–
90	3136	3	0.69	610	22	0.86	11967	–
180	2849	8	0.61	637	24	0.88	11557	–
0.4% Chloride								
7	1176	10	0.65	288	22	0.87	3282	–
30	1322	13	0.60	346	27	0.84	269	–
90	1542	6	0.73	227	55	0.73	5	19594
180	1991	5	0.71	302	98	0.66	0.4	6297
2% Chloride								
7	335	9	0.75	36	28	0.87	683	–
30	393	11	0.80	28	46	0.78	174	–
90	308	4	0.79	21	70	0.69	15	24416
180	389	5	0.81	28	94	0.64	4	8004

Table 6. Parameters used in the fitting of impedance data for low-nickel SS rebar embedded in mortar AAFA2.

Time Day	R_e Ω cm^2	$Y_{P_{HF}}$ μFcm^{-2}s$^{-(1-\alpha_{HF})}$	α_{HF}	R_{HF} Ω cm^2	$Y_{P_{LF}}$ μFcm^{-2}s$^{-(1-\alpha_{LF})}$	α_{LF}	R_{CT} kΩ cm^2
0% Chloride							
7	711	4	0.73	61	20	0.90	17534
30	802	6	0.72	82	19	0.90	15590
90	740	5	0.78	97	19	0.89	18110
180	727	9	0.71	119	20	0.88	22771
0.4% Chloride							
7	871	4	0.72	115	19	0.89	13866
30	1319	8	0.67	184	18	0.90	14140
90	807	5	0.74	120	18	0.89	16582
180	990	9	0.67	196	19	0.89	13210
2% Chloride							
7	390	5	0.72	49	19	0.87	5298
30	321	3	0.75	65	22	0.87	5807
90	682	13	0.69	61	19	0.87	4284
180	497	3	0.82	62	19	0.85	5325

Table 7. Parameters used in the fitting of impedance data for AISI 304 SS rebar embedded in mortar AAFA2.

Time Day	R_e $\Omega\ cm^2$	$Y_{P_{HF}}$ $\mu F cm^{-2} s^{-(1-\alpha_{HF})}$	α_{HF}	R_{HF} $\Omega\ cm^2$	$Y_{P_{LF}}$ $\mu F cm^{-2} s^{-(1-\alpha_{LF})}$	α_{LF}	R_{CT} $k\Omega\ cm^2$
0% Chloride							
7	703	11	0.65	78	25	0.90	12152
30	697	6	0.68	60	24	0.90	16134
90	733	2	0.87	59	25	0.90	10853
180	827	6	0.73	106	25	0.90	18865
0.4% Chloride							
7	696	14	0.59	107	19	0.91	49790
30	1198	9	0.68	132	19	0.91	28851
90	755	6	0.71	114	18	0.90	32950
180	1026	9	0.70	250	17	0.89	31504
2% Chloride							
7	345	16	0.69	31	17	0.92	23559
30	319	15	0.68	50	19	0.90	18049
90	349	7	0.84	43	17	0.90	29742
180	342	7	0.84	31	18	0.88	25309

Table 8. Parameters used in the fitting of impedance data for carbon steel rebar embedded in mortar AAFA2.

Time Day	R_e Ω cm^2	$Y_{P_{HF}}$ $\mu F cm^{-2} s^{-(1-\alpha_{HF})}$	α_{HF}	R_{HF} Ω cm^2	$Y_{P_{LF}}$ $\mu F cm^{-2} s^{-(1-\alpha_{LF})}$	α_{LF}	R_{CT} kΩ cm^2	Y_{0_W} Ω^{-1} cm^{-2} s$^{1/2}$
0% Chloride								
7	734	16	0.60	71	18	0.90	5858	–
30	801	10	0.66	92	18	0.89	7969	–
90	638	12	0.72	103	18	0.89	6765	–
180	531	8	0.77	73	18	0.88	7381	–
0.4% Chloride								
7	571	9	0.67	74	25	0.90	7118	–
30	768	10	0.61	105	22	0.89	5298	–
90	724	15	0.66	117	22	0.89	3332	–
180	685	5	0.75	102	25	0.90	8791	–
2% Chloride								
7	295	8	0.80	17	24	0.89	823	–
30	335	9	0.80	24	35	0.83	195	–
90	326	13	0.84	23	37	0.84	41	44778
180	485	13	0.81	33	54	0.82	2	22534